Lithological controls on light penetration into rock surfaces – implications for OSL and IRSL surface exposure dating

M.C. Meyer[1], L.A. Gliganic[1], M. Jain[2], R. Sohbati[2], D. Schmidmair[3]

[1] Institute for Geology, University of Innsbruck, 6020 Innsbruck, Austria
[2] Centre for Nuclear Technologies, Technical University of Denmark, DTU Risø Campus,
 DK-4000 Roskilde, Denmark
[3] Institute for Mineralogy and Petrography, University of Innsbruck, 6020 Innsbruck, Austria

Abstract

Luminescence surface exposure dating is a newly developed geochronological technique that allows the age of geological or archaeological rock surfaces to be accurately constrained. This dating method requires measuring and calibrating the depth-dependent luminescence signal below an exposed surface and relies on the assumption that neither the shape of the daylight spectrum nor the light attenuation change significantly with depth into the rock. However, lithologies with mm-scale heterogeneity in their mineral distribution or those lacking high sensitivity quartz present a challenge, partly because light attenuation with depth is not necessarily constant in such samples. Addressing these challenges is important for further development of the luminescence surface exposure dating technique.

Here we investigate the shape of luminescence-depth profiles in lithologies revealing complex fabrics such as coarse-grained granitic gneisses or gneisses with distinct planar metamorphic layering. We also present luminescence-depth profiles from quartzite, a lithology that appears – at first glance – highly homogenous. We find that the spatial distribution of opaque mineral phases in the metamorphic samples and precipitation of iron hydroxides in the quartzite strongly influence the 3-dimensional transparency and, consequently, the light attenuation with depth, and are the main cause for the observed scatter in the OSL- and IRSL-depth profiles in our samples. The data suggest that for rocks of heterogeneous lithology (i) close petrographic analysis of luminescence-depth profiles are required to ensure that the cores used for calibration have similar mineralogical composition (and thus light attenuation with depth) to those used to calculate a luminescence rock surface exposure age, and that (ii) RGB depth profiles appear to provide a useful semi-quantitative tool for such analysis.

1. Introduction

Luminescence dating is a well-established chronological technique normally applied to fine-grained (< 300 µm) sediments of clastic origin to estimate the time since sediment burial (e.g. Rhodes, 2011). Further development of this technique suggests that it can also be used to determine the exposure history of solid rock surfaces (e.g. Sohbati, 2015), which is based on the following principle: below a certain ambient temperature (i.e., closure temperature; e.g. Guralnik et al., 2015) latent luminescence begins to accumulate within the crystal lattice as a function of time due to the naturally occurring ionizing radiation inside rocks. Once the rock is exposed to daylight, e.g. due to erosion or transportation, this latent luminescence begins to gradually reset. The resetting (or bleaching) will eventually leave the topmost millimetres (typically < 20 mm) of a rock surface completely bleached. The rate of bleaching reduces systematically with depth (due to lower daylight intensity) to negligible values at depths where the luminescence signal is effectively unbleached and in field saturation. Given sufficient time, the profile reaches a secular equilibrium, where the rate of trapping due to ionising radiation becomes equal to the rate of detrapping due to daylight exposure at all depths. For a rock which is not in secular equilibrium, measuring and calibrating the depth-dependent luminescence signal below the exposed surface (via generating luminescence-depth profiles) allows – in principle – the exposure age of a geological or archaeological rock surface to be constrained (i.e. rock surface exposure dating; Polikreti, 2007; Sohbati et al., 2012a; Freiesleben et al., 2015). A related approach, known as rock surface burial dating, relies on the fact that upon burial, the luminescence signal in an already reset rock surface will accumulate again. Measurement of this re-accumulated latent luminescence (usually the signal from the top few mm of a surface) provides an estimate of the time since the surface was shielded from daylight (e.g. Greilich et al., 2005; Simms et al., 2011; Sohbati et al., 2015).

So far, three mineral-specific luminescence signals have been used as dosimetric signals in rock surface dating studies (see Sohbati, 2015 for a summary): (i) thermoluminescene (TL) from carbonate minerals, (ii) optically stimulated luminescence from quartz and (iii) infrared-stimulated luminescence from feldspar. The most promising results have been obtained using the OSL and IRSL signals from quartz and feldspar from relatively homogenous rock surfaces of sandstones, quartzite and granites, with relatively high luminescence sensitivities (Greilich et al., 2005; Vafiadou et al., 2007; Simms et al.,

2011; Chapot et al., 2012; Sohbati et al., 2012a, 2015; Simkins et al., 2013; Gliganic et al., 2018).

A mathematical model underlying the process of luminescence resetting with depth as a function of time in such homogenous lithologies has been introduced by Sohbati et al. (2011, 2012a, b). This function is used for estimating rock surface exposure time and includes parameters that describe (i) the wavelength-dependent daylight photon flux at the rock surface and the photoionization cross-section, (ii) light attenuation per unit depth (the attenuation factor μ, which is rock type dependent), and (iii) charge trapping probability (a function of dose rate and capture cross-section). For rock surface exposure dating this function must be calibrated via a known-age sample and further relies on the assumption that the attenuation factor μ can be treated as a constant, i.e. neither the shape of the daylight spectrum nor the light attenuation change significantly with depth into rock (Sohbati et al., 2012a).

In this contribution we investigate the shape of luminescence-depth profiles in complex lithologies characterized by a heterogeneous distribution of minerals on millimetre scale such as coarse-grained granitic gneisses or gneisses with a distinct planar metamorphic fabric. We contrast these observations with data from quartzite, i.e. a lithology that appears – at first glance – highly homogenous. We show that the spatial distribution of felsic and mafic minerals in the metamorphic samples and precipitation of iron hydroxides in the quartzite and granite gneiss samples strongly influence the 3-dimensional transparency and thus the attenuation factor μ. We discuss the implications of these new observations for accuracy and precision of optically stimulated luminescence (OSL) and infrared stimulated luminescence (IRSL) rock surface dating and consider potential solutions.

2. Samples and methods

Three samples ~20 x 15 x 10 cm in size with various degrees of metamorphic overprinting (see below) were obtained from the light-exposed surface of glacial boulders. These boulders were up to 2 m in diameter and sitting at the crest of a lateral moraine which formed during the glacial advance anno 1850 in the Hintertux valley (Eastern Alps). Geologically, the samples belong to the central gneiss unit of the Tauern Window, a metamorphic core complex and the highest section of the Eastern Alps (Oberhauser & Bauer, 1980). Samples HT-141 and 145 comprise coarse-grained granitic gneisses with weak metamorphic overprinting and quartz, K-feldspar, plagioclase and

mica (mainly biotite and phlogopit) as the main minerals. Zircons are concentrated within mica bands, while garnets occur accessorily (supplementary online material, SOM 1B, D). HT-144 is a gneiss sample with a strong planar fabric caused by alternating bands of quartz and feldspars (i.e. felsic minerals; light/translucent in colour) with dark minerals (i.e. mafic minerals – in this sample mainly biotite and phlogopit; SOM 1A). The metamorphic layering is laterally discontinuous (SOM 1C). Zircons and garnets occur accessorily but no accumulations of these mineral phases on the scale of the thin section were observed (SOM 1A).

Quartzite boulders from the southern Tibetan plateau (ca. 9.5 km southeast of the village of Lao Tingri) were also sampled and are almost entirely composed of ~100 – 300 μm large quartz crystals that show shadowy extinction under cross polarized light (Gliganic et al., 2018). Macroscopically, this lithology appears homogenous but on close examination some boulder surfaces and fractures show localised staining caused by crystallization of iron hydroxides (SOM 1E).

Under subdued red-orange light these rock surfaces were sampled either by using a water-cooled diamond coring drill to obtain cores of ~8 mm diameter and ~3 cm length or via a water-cooled stone saw to obtain blocks ~2 x 2 cm wide and ~3 cm long. These subsamples were cut precisely in 1 mm increments using a 0.3 mm thick diamond wafering blade mounted on a low-speed saw, yielding slices that were 0.7 – 0.9 mm thick. Different sample preparation procedures were followed to obtain the target aliquots for measurements: the 8 mm diameter slices were either measured as whole-rock slices or gently crushed in an agate mortar and sieved to obtain the 90-250 μm grain size fraction. Three small aliquots (each composed of ~500 grains) were measured per slice. The 2 x 2 cm slices were crushed and sieved to 90-250 μm and a sodium polytungstate solution with a density of 2.62 g/cm^3 was used to isolate heavy minerals and quartz from feldspar grains and the latter fraction was used for measurement (5 small aliquots per slice). Because of the small amount of material obtained from each crushed slice no further attempts were made to isolate Na-rich feldspar (plagioclase) from K-rich feldspar grains.

All luminescence measurements were made on a Risø TL/OSL reader (either model TL-DA 15 or 20). The feldspar-dominated metamorphic boulder samples were stimulated using IR LEDs (875 nm) and photons were detected using an Electron Tube Ltd 9635 photomultiplier tube through a Schott BG39 and Corning 7-59 filter set. The quartzite samples were stimulated using a post-IR OSL protocol that included a 100 s IR bleach at 50°C followed by blue LED OSL stimulation (470 nm), and the ultraviolet emission was detected through a 7.5 mm thick U-340 Hoya filter. Beta irradiations used

calibrated ^{90}Sr/^{90}Y sources mounted on the readers (Bøtter-Jensen et al., 2010). All thermal treatments and stimulations were done with a heating rate of 5°C s^{-1} and a pause of 14 s was inserted before optical stimulation to overcome thermal lag and allow all grains to reach the measurement temperature (Jain et al., 2007).

For quantifying the concentration of the main mineral, selected aliquots were pulverized subsequent to luminescence measurements and analysed using an X-ray powder diffractometer (XRD, type Bruker-AXS D8-Discover; ~5% precision on individual XRD measurements). Quantitative phase analysis of the X-ray powder patterns via the Rietveld method was performed with the software TOPAS Version 4.2 (Bruker-AXS, 2009) and included corrections of preferred orientation effects.

To investigate the colour variation (and by implication the rock transparency) in our samples, intact slices of selected cores were scanned at 1200 dpi resolution using an Epson GT 10000+ scanner and the average colour (RGB) value of each slice was extracted via the histogram function in Adobe Photoshop (CS4-extended). RGB versus depth profiles were constructed and compared with OSL- and IRSL-depth profiles.

3. Measurement protocols and data analysis

Aliquots obtained from the saturated inner part (depth > 25 mm) of the metamorphic boulders (HT-141, 144 and 145) yielded almost no blue-stimulated OSL signal but a bright response to stimulation with IR at 50°C for 100 s. This suggests the presence of insensitive quartz but high sensitivity Na- and/or K-feldspar grains and is in agreement with observations from other alpine catchments (Gliganic et al., 2017; Fuchs et al., 2013) as well as with investigations into the luminescence characteristics of crystalline rocks (e.g. Sohbati et al., 2011).

Dose recovery tests were conducted to investigate the dosimetric properties of the IRSL signal of the metamorphic boulders. For each sample 8 polymineral aliquots from crushed slices were prepared, bleached under a SOL 500 solar simulator at 120 cm distance for 1 hour. For 4 aliquots a dose of 18 Gy was administered, while for the remaining 4 aliquots the residual dose was determined. A single-aliquot regenerative dose (SAR; Murray and Wintle, 2000) procedure (200°C for 10 s natural/regenerative and test dose preheat with a 17.5 Gy test dose) was used to estimate the doses. For signal calculation the first 2 s minus a background integrated over the last 20.4 s of the signal were used. The dose recovery tests yielded ratios within 10% of unity (mean =

1.07±0.02) and residual doses that were generally less than 2 Gy (weighted mean = 1.3±0.03 Gy).

For the Tibetan quartzite samples, natural/regenerative and test dose preheats of 220°C for 10 s, stimulation temperature of 125°C, and an early-background subtraction signal integration approach were used. Experimental details are described by Gliganic et al. (2018).

For all samples, the sensitivity-corrected natural signals (L_n/T_n) from each slice were normalized to the corresponding core's saturation level. The normalization factor was the weighted mean value of the deepest five L_n/T_n values, showing a saturation plateau, typically at depths > 25 mm).

4. Results

4.1 IRSL-depth profiles from alpine metamorphic rock surfaces

A comparison between isochronous profiles, measured on crushed slices (Fig. 1a), crushed and density separated slices (to obtain feldspar extracts; Fig. 1b) and uncrushed slices (Fig. 1c) from the same surface of sample HT-144 reveal that the depth and shape of the bleaching front are highly variable depending on the exact location of the core. This variability does not seem to be dependent on the sample preparation technique (i.e. intact, crushed or crushed and density separated slices) (Fig. 1d).

For the granite gneiss samples HT-141 and HT-145 several of the IRSL-depth profiles from isochronous surfaces reveal unexpected scatter too: a discontinuous rise in the L_n/T_n signals with depth causes a stepped profile shape or local minima in the IRSL-depth profiles that would otherwise reveal rather sigmoidal shape. Such unexpected curve features are evident in the IRSL-depth profiles of the cores 1 and 5 from sample HT-141 (Fig. 1e; both measured on crushed slices) and in the cores 1 and 4 from sample HT-145 (the former was measured on intact slices while the latter on crushed slices; Fig. 1f). The resulting IRSL-depth profile measured on the feldspar fraction is smoother than the profile constructed from crushed material without any separation (HT- 141 core 5), but is still stepped (Fig. 1e).

4.2 IRSL-depth profiles and mineralogical composition

For the crushed slices of HT-141 A core 1 and of HT-144 A2 and A4 the mineralogical composition of each slice was determined using XRD. The XRD data and

the IRSL-depth profiles are shown in Figure 2a and b for the samples HT-141 (core 1) and HT-144 (blocks A2 and A4), respectively. For HT-141 A core 1 the concentration of K-feldspar and plagioclase co-varies down profile (in the 10-50% margin), while quartz is anti-correlated with the feldspar concentration. The mafic mineral concentration in this core is generally low (< 10%) with one peak (13%) immediately preceding a distinct local minimum of the IRSL-depth profile. This local minimum is mimicked by the feldspar curve and coincides with a local peak in the quartz concentration (Fig. 2a).

Only the slices between 4.5 and 7.5 mm depth of the IRSL-depth profiles HT-144 A2 and A4 (from an isochronous surface) were analysed using XRD. Over this depth interval the bleaching fronts of these IRSL profiles are farthest from each other. The ratio between K-feldspar and plagioclase remains broadly constant for each depth and curve (Fig. 2b). Over the same depth interval almost no variation in the concentration of quartz and mafic minerals is observed in the two cores.

4.3 OSL-depth profiles for Tibetan quartzite surfaces

For the Tibetan quartzite, OSL-depth profiles were constructed from three rock surfaces that have each been exposed to daylight for exactly 20 months. These fresh surfaces were created in the field by chiselling off the previously light-exposed part of large quartzite boulders (of identical lithology) and sampled 20 months later. For each of these artificially-created rock surfaces two cores were drilled, sliced, measured, and after shown to be reproducible, combined to construct a sample-specific OSL-depth profile. Despite the isochronous nature of these surfaces, the depth of the bleaching front in the OSL-depth profiles defined as the depth of the inflection point varies significantly (between 4 and 15 mm; Fig. 3d).

4.4 Comparison of IRSL and OSL-depth profiles with RGB profiles

RGB values obtained via spot measurements in Adobe Photoshop for very dark (black) areas that are dominated or entirely composed of mafic minerals such as biotite vary from 0 to 5. For samples HT-145, TIN-099 and TIN2016-150 oxidation has resulted in orange-brownish staining of some or all slices. Thus, the most intensively-stained areas from these samples attain RGB values of 0 to 5 too. RGB spot measurements for quartz- and feldspar-dominated areas vary from 150 to160 and from 200 to 235, respectively (SOM 1F to K). The average RGB value of each slice is plotted down-core and compared with the luminescence-depth profiles for three samples in Figure 3. Those IRSL-depth profiles of sample HT-144 that reach saturation at a shallower depth (within ~6 to 7 mm)

have dark to very dark surface slices (e.g. the RGB value of 57 of core 2 is one of the lowest in the entire dataset; SOM 1F) and steep and abrupt increases in L_n/T_n values that coincide with very low RGB values (Fig. 3a). In contrast, profiles with L_n/T_n saturation attained at $\geq$ 13 mm depth show RGB values $\geq$ 100 for the surface slices and the entire depth range prior to saturation (Fig. 3b).

The individual RGB profiles for the isochronous surface HT-145 show comparatively little internal variability. For the unsaturated part of the IRSL-depth profiles RGB values fluctuate around 130 (core 3) and 90 (core 1), while the corresponding IRSL-depth profiles are of broadly similar shape and reach saturation at ~12 mm depth.

For the Tingri samples the core with the lowest average RGB value saturates closest to the surface (TIN-150: average RGB 108, saturation at ~4 mm depth), while cores with lighter colours saturate in sequentially greater depths (Fig. 3d). Furthermore, an abrupt increase in the L_n/T_n values of core TIN-150 coincides with a strongly decreasing RGB trend (at 3 mm depth; Fig. 3d), which is associated with a yellow to brownish zone caused by iron hydroxides.

5. Discussion

Sensitivity analyses of the bleaching-with-depth model of Sohbati et al. (2012a) suggest that the bleaching front and shape of isochronous luminescence-depth profiles is strongly dependent on the effective detrapping rate of the luminescence at the rock surface (their $\overline{\sigma\varphi_0}$ parameter) and the (rock type specific) attenuation factor μ, respectively. Because we are comparing luminescence-depth profiles obtained from individual isochronous surfaces with each other, the $\overline{\sigma\varphi_0}$ parameter for each surface must be identical. Thus, the observed variability across different cores may arise from factors such as variable mineralogy of luminescent phases, different dose rates, and/or differential light penetration (i.e. rock transparency) and is explored in the following.

5.1 Variable mineralogy and luminescence origins and differential dose rates

To investigate the source of discrepancy between the IRSL-depth profiles from isochronous surfaces, we first tried to avoid IRSL signal contamination from potentially luminescent mica (Kortekaas and Murray, 2005; Clark and Sanderson, 1994) or heavy mineral grains (Jain et al., 2006; Turkin et al., 2006) by constructing IRSL-depth profiles using purified feldspar extracts (by crushing and density separation of 2 x 2 cm slices).

However, the density separated feldspar extracts still yielded highly scattered IRSL-depth profiles. This was also the case when intact rock slices were measured (Fig. 1).

It has been demonstrated that the IRSL signal stability among different types of feldspar can differ, especially when low preheat temperatures are applied (< 320 °C; Li and Wintle, 1992; Thiel et al., 2011; Tsukamoto et al., 2012). IRSL-depth profiles in our study were measured at 50 °C after preheating to 200 °C and Na- and K-feldspar grains are visible in all thin sections of the metamorphic samples (SOM 1). Hence, scatter in some of the IRSL-depth profiles (local minima of surface HT-141 or differential bleaching depths of surface HT-144) could, in principle, result from slices that are either dominated by Na- or K-feldspar, and thus suffer from anomalous fading to different degrees. However, the XRD analyses reveal that the ratio of Na- to K-feldspar of individual slices (Fig. 2a) as well as between adjacent slices from the same depth (Fig. 2b) does not vary significantly (with the only exception being the two slices at 4.5 mm depth in Fig. 2b). Differences in feldspar fading rates along the cores are thus an unlikely explanation for the observed scatter in the IRSL-depth profiles and cannot explain the differences in OSL-depth profiles of the TIN samples either.

Thin sections from the granite gneiss samples showed concentration of zircons in mica bands, which could act as local dose rate hotspots and be responsible for local L_n/T_n maxima such as those observed at ~18 mm and 23 mm in HT-141 core 1 (Fig. 1e; SOM A). Correction for any hypothetical zircon hotspots would drag the local minima/maxima further down, which would take the isochronous profiles of sample HT-141 (core 1, core 5, B2; Fig. 1e) farther apart from each other (instead of lining them up). We therefore regard the zircon hotspot hypothesis as a less likely explanation for the observed local minima/maxima in the profiles. Furthermore, in thin sections of sample HT-144 zircon concentrations are absent (SOM B), but this sample reveals even larger scatter in the IRSL-depth profiles compared to HT-141 (Fig. 1d, e).

5.2 Rock heterogeneity, rock transparency and the attenuation coefficient (μ)

In this study, RGB profiles are used as proxy for rock transparency down-core. We find that high concentrations of opaque (i.e. mafic or strongly oxidized) minerals in the metamorphic and quartzite samples are responsible for low average RGB values in the measured slices. We suggest that these opaque mineral phases strongly influence the light penetration into the rock surfaces by (i) exerting a strong control on the position of the bleaching front into a sample surface (i.e. darker cores from isochronous surfaces consistently reveal shallower bleaching fronts; Fig. 3a, b, d) and (ii) influencing the slope

of the OSL- and IRSL-depth profiles in our samples (L_n/T_n values increase significantly where transparency decreases; Fig. 3a and core TIN2016-150 in Fig. 3d). In a similar manner, the particularly dark surface slice of core 2 of sample HT-144 seems to block light penetration into the rock resulting in a very shallow bleaching front of the corresponding IRSL-depth profile (Fig. 3a). The effect of lithological control on light penetration should be most pronounced in samples with high transparency contrasts, such as (i) the Tibetan quartzite, where formation of iron hydroxides of highly translucent quarzitic groundmass can change the overall colour hue of the sample or form opaque patches or layers, and (ii) samples with a distinct metamorphic layering like HT-144.

For the isochronous surface HT 144 we further explore the relation between depth of the bleaching front, average RGB value and the attenuation coefficient, μ. We use the five cores of sample HT 144 for which both, IRSL-depth and RGB profiles are available (plotted in Fig. 3a to b) and perform a global fit to the L_n/T_n profiles of the bleaching with depth model (equation 1 in Sohbati et al., 2012a). Because all IRSL-depth profiles of HT 144 are from an isochronous surface, they share the value of $\overline{\sigma\varphi_0 t}$. This allows us to estimate the value of μ for each IRSL-depth profile. The obtained values range between 1.10 (HT144 slab C core 2) and 0.44 (HT144 slab C core 3). For each luminescence profile we also calculated (i) the depth of the bleaching front (defined as the depth of inflection, i.e. where the Ln/Tn curve obtains ~50% of saturation) and (ii) the average RGB value before the inflection point (as an approximation for the profile specific average rock transparency). Figures 4a and b show that the relation between the modelled attenuation coefficient μ and the depth of inflection (bleaching front) and between μ and the average RGB value before inflection (rock transparency) are broadly linear, at least for average RGB values > 150. The same applies to the relation between depth of inflection and average RGB before inflection (Figure 4c).

The opaque mineral phases in the granite gneiss samples HT-141 and 145 form large aggregates of ~1 cm in diameter, which occur in patches rather than distinct planar layers as is the case in sample HT-144 (SOM A-C). We argue that the scatter in IRSL-depth profiles in these samples (local L_n/T_n minima/maxima; Fig. 1e, f) may be explained by these mafic patches "shadowing" the constituent mineral grains, and that deeper grains may be more bleached by light "piping" around the mafic patches. This interpretation is supported by the XRD data, RGB data, and the luminescence-depth profile of HT-141 core 1, HT-145 2 core 1, and TIN-150, where higher concentrations of opaque minerals are preceding or coinciding with local minima and/or kink-like steps observed in the luminescence-depth profiles (Fig. 2a and 3c, d).

Our results suggest that highly heterogeneous lithologies should be approached with caution for OSL rock surface exposure dating due to likely variations in the value of μ in samples with high transparency contrasts arising from features such as planar metamorphic fabrics with mafic and felsic mineral phases. Even for homogenous, resistant lithologies such as quartzite the difference between isochronous OSL-depth profiles can be significant because of weathering and precipitation of iron hydroxide that can differentially penetrate into rock surfaces and, thus heterogeneously altering the attenuation factor μ.

Our data also suggest that for OSL rock surface exposure dating scale relations between sampling size (e.g. coring diameter) and the dimensions of lithological heterogeneities should be considered. For example, ~8.5 mm diameter cores are sufficient for measuring reproducible OSL-depth profiles from samples of a homogeneous lithology (e.g., TIN samples). By contrast, while the detrimental effects (local minima/maxima in the L_n/T_n curves) caused by the ~10 mm mafic patches are obvious in the IRSL-depth profiles constructed from HT 141 A core 1 and 5 (core diameters ~ 8 mm; Fig. 1e), they are almost absent in the IRSL-depth profile of the same surface constructed from sliced blocks with a base area of 200 x 200 mm (HT 141 B2, Fig. 1e). The larger sampling scheme resulted in an increase in sample volume by a factor of ~8 in the blocks compared to the cores and significantly improved the reproducibility of the IRSL-depth profiles for the granitic samples HT 145 and HT 141. However, in the case of the pervasive metamorphic layering of sample 144, IRSL-depth profiles constructed from sliced blocks did not remove any of the observed scatter in the depth of the IRSL bleaching fronts (Fig. 1a-c). This suggests that averaging multiple cores (≤ 1 cm diameter) from isochronous surfaces of granitic samples showing small-scale granular heterogeneities likely improves the accuracy of luminescence depth profiles, while samples with a distinct and pervasive metamorphic layering such as HT 144 may not be suitable for OSL surface exposure dating, using current preparation techniques (at least as long as the sampling direction is perpendicular to the metamorphic layering).

Many earth surface processes that are datable using OSL rock surface exposure dating technique (e.g. rock falls or the evolution of head scarps of deep-seated landslides) have a structural constraint and many mass movements are actually formed along and parallel to such planar metamorphic fabrics. In homogenous lithologies, well suited for OSL rock surface dating, staining and chemical alterations are often small-scale and difficult to recognize by simple visual inspection. Hence, identifying and addressing such

effects seems to be necessary for applying OSL rock surface dating to a wide range of crystalline rock types in earth surface and archaeological studies.

In summary, we find that the spatial distribution of opaque mineral phases on the mm- to sub-mm scale is the main cause for the observed scatter in the OSL and IRSL-depth profiles in our samples and is responsible for the apparent variation of µ across a given surface . We found this effect to be most pronounced in quartzite that – at first sight – appears highly homogenous and translucent but suffers from weathering and the differential formation of yellow iron oxides, and in gneiss with distinct planar metamorphic layering. Because the fabric of many metamorphic and igneous rocks is heterogeneous on the cm- to sub-mm scale, light "piping" into such rock surfaces will depend on the exact 3D geometry of opaque versus translucent mineral phases and is potentially complex. We suggest that for heterogeneous lithologies OSL rock surface dating may be applicable by pooling only those luminescence-depth profiles for age calculation showing broadly comparable RGB profiles, and thus ensuring inter- and intra-sample consistency in µ value between isochronous depth profiles and calibration samples (e.g. all cores from Fig. 3b). A next step into this direction might involve slice- or even mineral specific quantitative transparency measurements.

5. Conclusions

We conclude that a heterogeneous distribution of opaque minerals can significantly affect the reproducibility of luminescence-depth profiles. While such heterogeneity is expected in coarse, polymineralic rocks (e.g. planar metamorphic or granitic fabrics with mafic and felsic mineral phases), we demonstrate that it can also be present in homogeneous single phase rocks such as quartzite. Our data demonstrate the need for close petrographic analysis of luminescence-depth profiles to ensure that the cores used for calibration have similar mineralogical composition (and thus µ) to those used to calculate an OSL rock surface exposure age. Easy-to-measure RGB depth profiles appear to provide a useful semi-quantitative tool for such analysis. This has important implications for age calibration in surface exposure dating.

References

Bøtter-Jensen, L., Thomsen, K.J., Jain, M., 2010. Review of optically stimulated luminescence (OSL) instrumental developments for retrospective dosimetry. Radiat. Meas. 45, 253–257. doi:10.1016/j.radmeas.2009.11.030

Bruker-AXS: TOPAS Version 4.2: General Profile and Structure Analysis Software for Powder Diffraction Data., Bruker-AXS, Karlsruhe, Germany, 2009.

Buylaert, J.-P., Jain, M., Murray, A.S., Thomsen, K.J., Thiel, C. and Sohbati, R., 2012. A robust feldspar luminescence dating method for Middle and Late Pleistocene sediments. Boreas 41 (3):435-451. 03009483.

Chapot, M.S., Sohbati, R., Murray, A.S., Pederson, J.L. and Rittenour, T.M., 2012. Constraining the age of rock art by dating a rockfall event using sediment and rock-surface luminescence dating techniques. Quaternary Geochronology 13, 18-25.

Clark, R.J., Sanderson, D.C.W., 1994. Photostimulated luminescence excitation spectroscopy of feldspars in micas. Radiation Measurements 23, 641e646.

Fuchs, M.C., Böhlert, R., Krbetschek, M., Preusser, F. and Egli, M., 2013. Exploring the potential of luminescence methods for dating Alpine rock glaciers. Quaternary Geochronology 18, 17-33.

Gliganic, L.A., Cohen, T.J., Meyer, M. and Molenaar, A., 2017. Variations in luminescence properties of quartz and feldspar from modern fluvial sediments in three rivers. Quaternary Geochronology 41 70-82. 1871-1014.

Gliganic, L.A., Meyer, M.C., Sohbati, R., Jain, M., 2018. OSL surface exposure dating of a lithic quarry in Tibet: laboratory validation and application. Quaternary Geochronology – special issue related to the LED Cape Town, September 2017, submitted.

Greilich, S., Glasmacher, U.A. and Wagner, G.A. (2005): Optical dating of granitic stone surfaces. Archaeometry 47, 645-665.

Guralnik, B., Jain, M., Herman, F., Paris, R. B., Harrison, T. M., Murray, A. S., Pierre G. Valla, and Rhodes, E. J. (2013). Effective closure temperature in leaky and/or saturating thermochronometers. Earth and Planetary Science Letters, 384, 209-218.

Jain, M., Andersen, C.E., Bøtter-Jensen, L., Murray, A.S., Haack, H. and Bridges, J.C., 2006: Luminescence dating on Mars: OSL characteristics of Martian analogue materials and GCR dosimetry. Radiation Measurements 41, 755-761.

Jain, M., Bøtter-Jensen, L., Murray, A. S., & Essery, R. (2007). A peak structure in isothermal luminescence signals in quartz: Origin and implications. Journal of luminescence, 127(2), 678-688.

Kortekaas, M., Murray, A., 2005. A method for the removal of mica from quartz separates. Ancient TL 23, 43e46.

Li, S.-H., Wintle, A.G., 1992. A global view of the stability of luminescence signal from loess. Quaternary Science Reviews 11, 133-137.

Liritzis, I. (2011): Surface dating by luminescence: an overview. Geochronometria 38, 292-302.

Oberhauser, R., Bauer, F. K., & Bundesanstalt, G. (Eds.)., 1980. Der geologische Aufbau Österreichs. Springer-Verlag.

Polikreti, K. (2007): Detection of ancient marble forgery: techniques and limitations. Archaeometry 49 (4):603-619.

Rhodes, E.J. (2011): Optically Stimulated Luminescence Dating of Sediments over the Past 200 000 Years. Annual Review Earth and Planetary Sciences 39, 461-488.

Simms, A.R., DeWitt, R., Kouremenos, P. and Drewry, A.M., 2011. A new approach to reconstructing sea levels in Antarctica using optically stimulated luminescence of cobble surfaces. Quaternary Geochronology 6 (1):50-60. 1871-1014.

Simkins, L.M., Simms, A.R. and DeWitt, R., 2013. Relative sea-level history of Marguerite Bay, Antarctic Peninsula derived from optically stimulated luminescence-dated beach cobbles. Quaternary Science Reviews 77 (0):141-155. 0277-3791.

Sohbati, R., Murray, A., Jain, M., Buylaert, J.-P. and Thomsen, K. (2011): Investigating the resetting of OSL signals in rock surfaces. Geochronometria 38, 249-258.

Sohbati, R., Murray, A. S., Chapot, M. S., Jain, M., and Pederson, J., (2012a): Optically stimulated luminescence (OSL) as a chronometer for surface exposure dating. Journal of Geophysical Research, 117, B09202.

Sohbati, R., Jain, M. and Murray, A. (2012b) Surface exposure dating of non-terrestrial bodies using optically stimulated luminescence: A new method. Icarus 221 (1):160-166. 0019-1035.

Sohbati, R., Murray, A.S., Porat, N., Jain, M. and Avner, U., 2015. Age of a prehistoric Rodedian cult site constrained by sediment and rock surface luminescence dating techniques. Quaternary Geochronology 30, Part A 90-99.

Sohbati, R. (2015): Luminescence, rock surfaces. In: Encyclopedia of Scientific Dating Methods, pp. 485-488. Springer

Thiel, C., Buylaert, J.-P., Murray, A., Terhorst, B., Hofer, I., Tsukamoto, S. and Frechen, M., 2011. Luminescence dating of the Stratzing loess profile (Austria) - Testing the potential of an elevated temperature post-IR IRSL protocol: Loess in Eurasia. Quaternary International 234, 23-31.

Tsukamoto, S., Jain, M., Murray, A., Thiel, C., Schmidt, E., Wacha, L., Dohrmann, R. and Frechen, M., 2012. A comparative study of the luminescence characteristics of polymineral fine grains and coarse-grained K-and Na-rich feldspars. Radiation measurements 47, 903-908.

Turkin, A.A., Vainshtein, D.I. and Den Hartog, H.W., 2006. Modelling of Optically Stimulated Luminescence of Zircon: Assessment of the Suitability for Dating. Journal of Physics D-Applied Physics 39, 1367-1377.

Vafiadou, A., Murray, A. and Liritzis, I., 2007. Optically stimulated luminescence (OSL) dating investigations of rock and underlying soil from three case studies. Journal of Archaeological Science 34 1659-1669.

Figure Captions:

Figure 1: IRSL-depth profiles for the gneiss sample HT-144 (a-d) and the granitic gneiss samples HT-141 (e) and HT-145 (f). The IRSL-depth profiles in (a) were constructed based on aliquots from crushed slices (~8 mm diameter) with each data point being the weighted mean of three aliquots; in (b) a block with a base area of 200 x 200 mm was sliced and the crushed slices were density separated and feldspar extracts measured (weighted mean of five aliquots per slice and data point); in (c) intact (uncrushed) slices (~8 mm diameter) were measured. Figure (d) shows all IRSL-depth profiles of sample HT-144 on a semi-log scale. The IRSL-depth profiles of sample HT-141 (e) are based on crushed slices (3 aliquots per slice and data point) and feldspar extracts (5 aliquots per slice and data point). The IRSL-depth profiles of sample HT-145 (f) are based on intact slices and crushed slices (3 aliquots per slice and data point; compare legend).

Figure 2: Comparison of IRSL-depth profiles and quantitative mineralogical composition for the granite gneiss samples HT-141 (a) and the gneiss sample HT-144 (b). For the mineralogical analysis each slice was pulverized subsequent to IRSL measurements and measured via XRD. The grey box in (b) indicates the depth interval over which XRD measurements were made.

Figure 3: Comparison of luminescence-depth profiles with RGB profiles for the gneiss sample HT-144 (a, b), the granite gneiss sample HT-145 (c) and the quartzite (TIN) samples (d). Note that the RGB axis is covering a range from 0 (black) to 255 (white). The RGB profiles are based on slices that were scanned after IRSL measurements and each data point is the average RGB value per slice.

Figure 4: Relation between (a) the attenuation coefficient μ and the depth of inflection or bleaching front and (b) between μ and the average RGB value before inflection, the latter being a proxy for rock transparency. In (c) the relation between depth of inflection and average RGB before inflection is plotted.
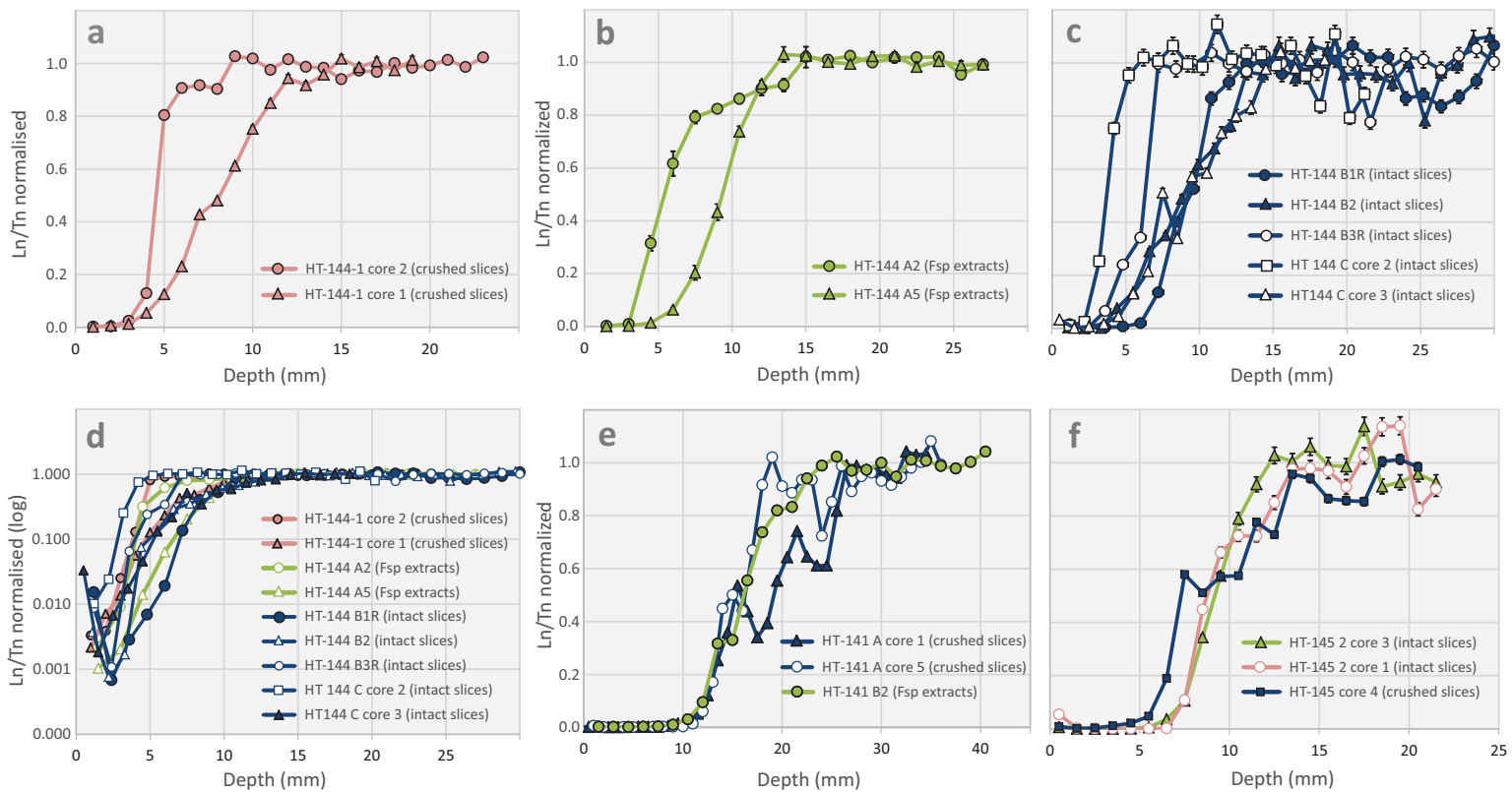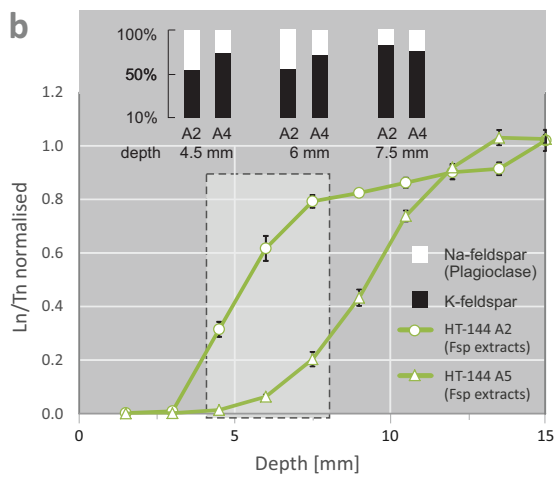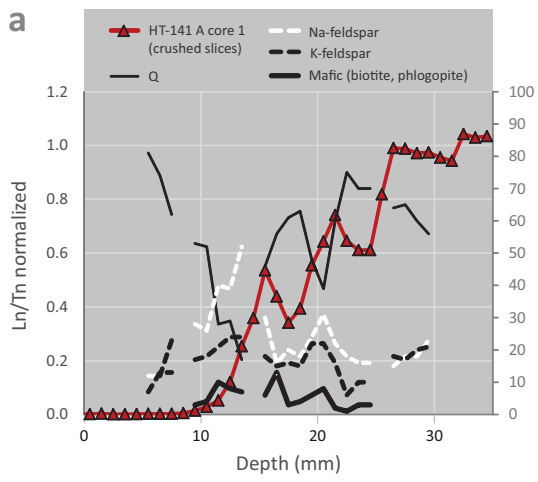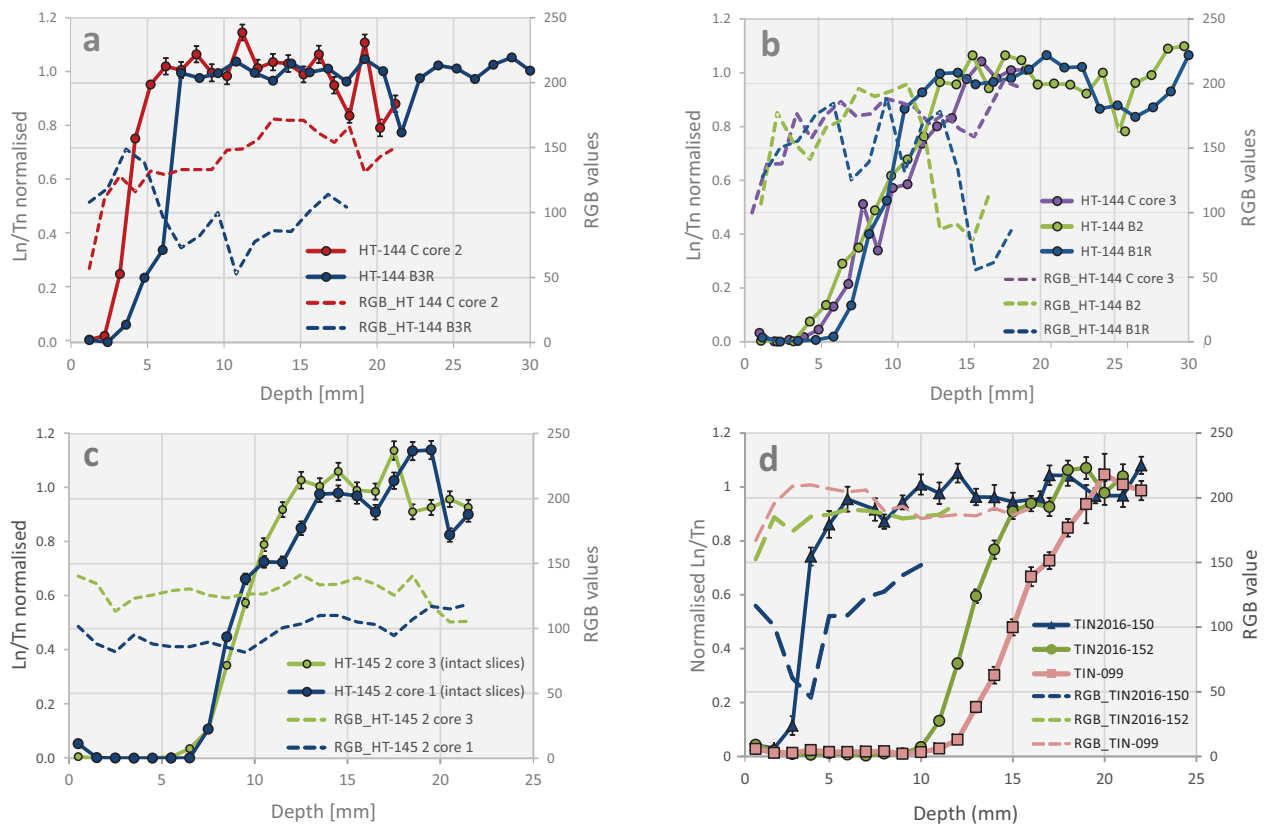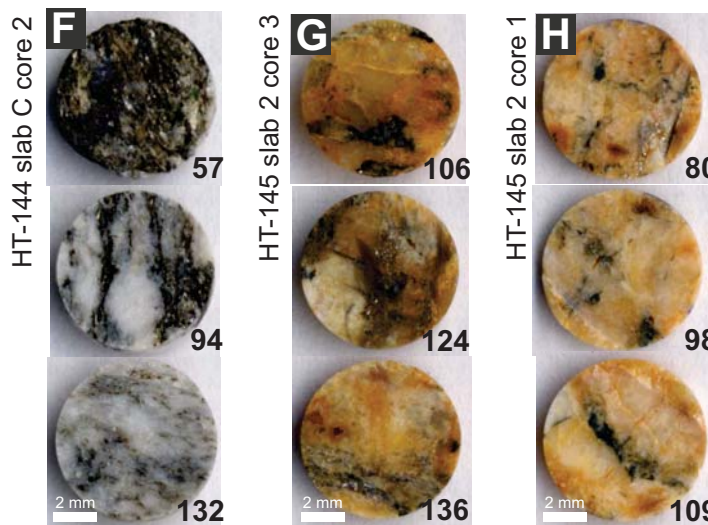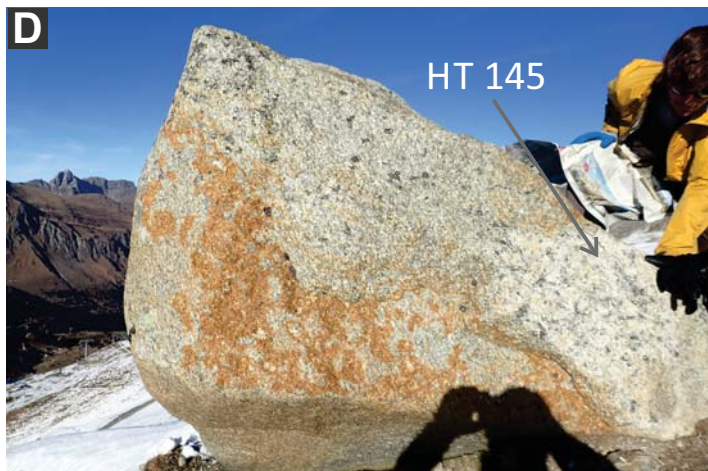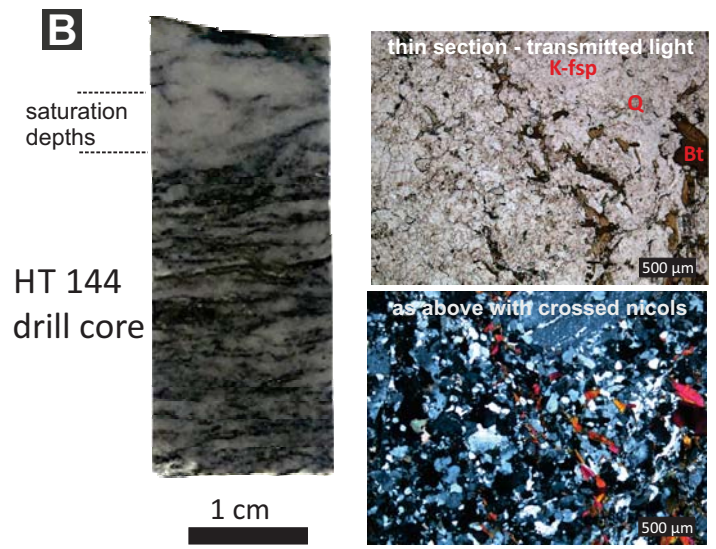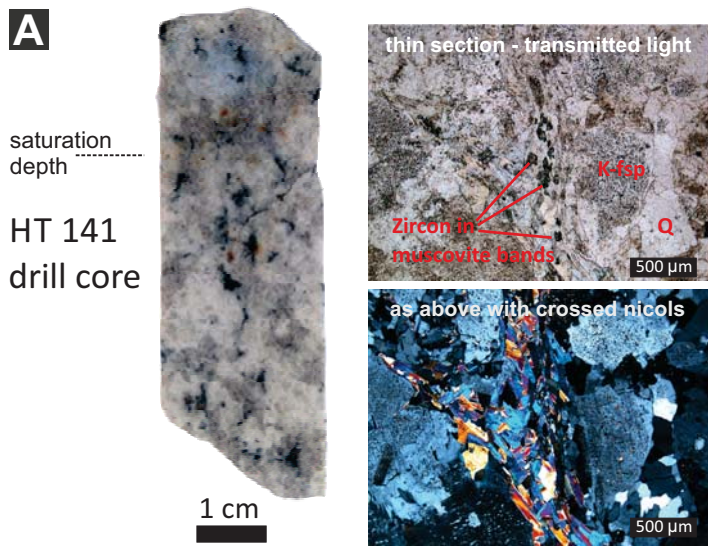
Figure 1

Figure 2

Figure 3
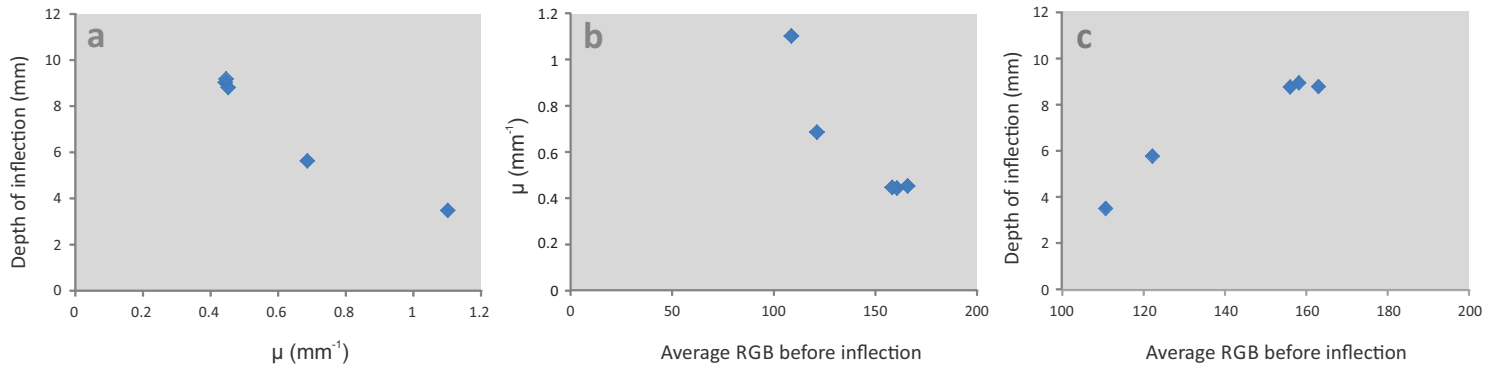
Figure 4
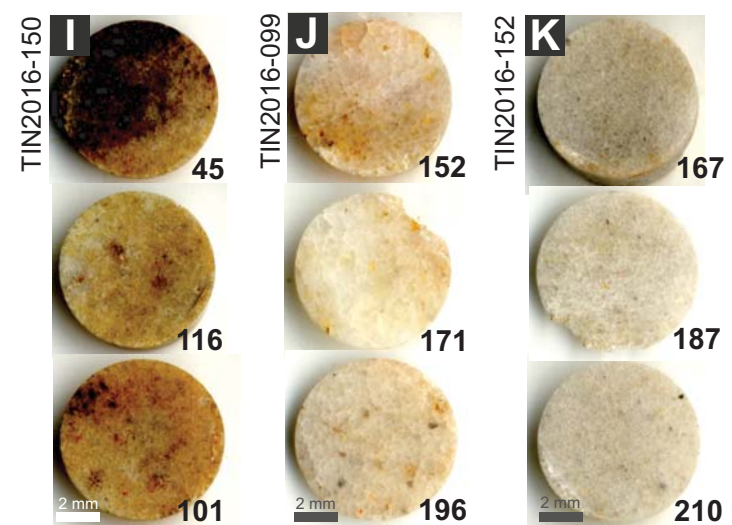
Supplementary online material 1: Samples HT-141 (A) and HT-145 (D) are granitic gneisses with weak metamorphic overprinting and mafic (opaque) minerals arranged in mm aggregates. B & C: HT-144 is a gniss with strong planar fabric formed by quartz-feldspar bands alternating with mafic bands. E: Quartzite boulder with partially stained surface (reddish, upper part of image); sample TIN2016-099 was taken next to the compass. F-K: Optical images of slices from unsaturated part of luminescence-depth profiles of selected cores. The average RGB value for each slice is indicated (lower right corner). The slices are sorted according to their RGB value: top row = darkest slices (lowest RGB value from unsaturated part of each profile); bottom row = brightest slice (highest RGB value); middle row = median slice (RGB value).